J. Fluid Mech. (1996), *vol.* 306, *pp.* 43–57

Interaction of oblique shock waves and planar mixing regions

By D. R. BUTTSWORTH†
Department of Mechanical Engineering, University of Queensland, Australia

(Received 2 December 1994 and in revised form 21 August 1995)

An analysis for predicting the interaction of a steady oblique shock wave and a planar mixing region is presented. Specifically, an equation for the shock curvature was obtained from the shock wave and isentropic wave difference equations which govern the shock transmission within a region of varying Mach number. The effects of non-uniform gas composition within the mixing region were assessed using a similar treatment; however, the wave equations were expanded in terms of a varying ratio of specific heats instead of a varying Mach number. An expression for the shock-induced vorticity due to velocity and density gradients within the mixing region was also obtained. This expression provides a means of estimating the possible mixing augmentation induced in various shock wave–mixing region interactions. When the velocity and density gradients within the mixing region oppose each other, it is demonstrated that the pre-shock vorticity may be attenuated by the shock. Applications of the analysis are discussed with reference to specific examples involving mixing augmentation and shock oscillation.

1. Introduction

Mixing between fuel and air streams under highly compressible conditions, such as occur in a supersonic combustion ramjet (scramjet) engine, is inherently slow. In order to enhance the mixing rates (and thereby produce a more efficient engine), reliable mixing augmentation techniques must be developed. A number of candidate methods are currently being investigated.

A variety of bluff and streamlined bodies and geometries have been used in attempts to destabilize the fuel–air mixing region and induce large-scale vorticity (Guirguis 1988; Northam *et al.* 1991; Roy 1991; Tillman, Patrick & Paterson 1991; Fernando & Menon 1993). Attempts have been made to optimize the injection configuration by (i) using different jet cross-sections (Schadow, Gutmark & Wilson 1990); (ii) altering the fuel injection angle (Northam & Anderson 1986); and (iii) utilizing multiple points of injection. Pulsed injection has also been used in attempts to achieve faster mixing (Randolph, Chew & Johari 1994). Pressure mismatching between the fuel and air streams has been examined (Sullins *et al.* 1991; Hall, Dimotakis & Roseman 1993) and under certain conditions mixing augmentation has been observed (Gilreath & Sullins 1989). Li, Kailasnath & Book (1991) examined the possibility of using expansion waves to enhance mixing in co-flowing supersonic streams. Currently, *shock* impingement appears an attractive candidate for mixing enhancement due, in part, to the inherent presence of shock waves within the intake and combustor regions of scramjet engines.

† Present address: Department of Engineering Science, University of Oxford, Parks Road, Oxford OX1 3PJ, UK.

Varying degrees of shock-induced mixing augmentation have been observed experimentally. Marble, Hendricks & Zukoski (1987) and Marble *et al.* (1990), utilized an oblique shock to enhance the mixing rate of circular jets in a co-flowing air stream. Mixing enhancement was also demonstrated by Menon (1989) using shock impingement on a mixing region formed between a sonic helium jet and a supersonic nitrogen stream. Hyde *et al.* (1990) also observed shock-induced mixing enhancement in their wall slot injection studies. Shock impingement was used by Waitz, Marble & Zukoski (1993) in a contoured wall injector configuration in an attempt to enhance the mixing and penetration of the jets. Axial vorticity was induced through the shock interaction; however, additional vorticity sources which also enhanced the mixing were present. Accelerated mixing was observed by Shau, Dolling & Choi (1993), but only at locations close to the shock wave; further downstream, the mixing rate relaxed to the undisturbed value.

A number of numerical studies investigating shock-augmented mixing have recently been conducted. Kumar, Bushnell & Hussaini (1989) used an Euler code to study the conversion of the mean flow energy into fluctuating energy by modelling an oscillating shock wave such as may arise due to boundary layer separation in a compression corner. Yang, Kubuta & Zukoski (1993) examined the unsteady interaction of an imbedded gas cylinder and a normal shock wave and thereby gained insight into the analogous steady problem, namely the interaction of an oblique shock and a circular fuel jet. The interaction of an oblique shock and circular fuel jet was studied directly by Drummond (1991) using a Navier–Stokes solver. He observed greatly enhanced mixing due to the streamwise component of vorticity that was added to the jet through the interaction process. In another numerical study, Vasilev *et al.* (1994) observed mixing enhancement factors of between 2 and 4 when single oblique shock waves interacted with square mixing jets.

Analytical approaches relevant to the study of shock wave–mixing region interactions have also been developed. Calculations based on analytical models of shock wave–turbulence interactions indicate that varying degrees of turbulence generation and amplification are possible, depending on the actual system (e.g. Morkovin 1960; McKenzie & Westphal 1968; Anyiwo & Bushnell 1982; Ribner 1987). Using a linearized approach, Riley (1959) modelled steady flow features associated with the impingement of an oblique shock wave on a boundary layer. Henderson (1967) examined the steady features of shock wave–boundary layer interactions by approximating the boundary layer profile with incremental Mach number steps and solving the wave equations governing the shock transmission at each step. Roshko & Thomke (1970) also modelled the boundary layer as an inviscid region of vortical flow; compression corner pressure distributions were successfully predicted using a method of characteristics solution.

The current modelling of the shock wave–mixing region interaction is similar to that adopted by Henderson (1967). However, instead of simultaneously solving the governing wave equations at incremental steps in the Mach number distribution, the wave equations are expanded in difference form to give a differential equation for the shock trajectory due to a continuously varying Mach number region. Having established the relationship between the shock curvature and the Mach number gradients, an expression for the post-shock vorticity is then obtained. The present analysis provides a means of rapidly estimating the changes in the large-scale vorticity due to the steady interaction of an oblique shock wave and a planar mixing region. It may be possible to infer the shock-induced changes in the mixing rate which persist after unsteady mixing enhancement effects have decayed using the present vorticity results.

2. Modelling the interaction process

2.1. *Effects of a non-uniform Mach number distribution*

Consider the situation depicted in figure 1. The incident shock wave is assumed to be a steady oblique shock wave generated by a flat plate. In the region upstream of the shock wave, the flow is assumed to be parallel, free from all pressure gradients, and is initially characterized by a steady transverse variation in Mach number alone. The shock does not decelerate the flow to subsonic speeds. A perfect gas with a constant value of γ is assumed to exist throughout the flow field, although the composition of the flow is not necessarily uniform. Figure 1 depicts a flow in which there is a step in the Mach number distribution; however, the limit $\delta M_1 \to 0$ will be taken. That is, a solution for a continuous variation in pre-shock Mach number is sought. When $M_1(y)$ is continuous, the waves initially reflected will be isentropic.

Transmission and reflection of the incident shock wave will be such that on either side of the dividing streamline, the flow will have the same pressure and be moving in the same direction (see figure 1). Conditions of matched deflection and pressure are given by

$$\delta\omega = -\delta\zeta_r, \tag{1}$$

$$\delta p_4 = \delta p_3. \tag{2}$$

Assuming that the region into which the incident wave is transmitted has the same γ as the initial region, the pressure change across the transmitted wave can be obtained from the Rankine–Hugoniot shock relations (Liepmann & Roshko 1957) as

$$\frac{\delta p_4}{p_1} = \frac{4\gamma}{\gamma+1}(M_1 \sin^2\theta\,\delta M_1 + M_1^2 \sin\theta\cos\theta\,\delta\theta) \tag{3}$$

once second-order terms in δM_1 and $\delta\theta$ are neglected. To a similar approximation, the shock relation for the flow deflection through the transmitted oblique shock wave gives

$$(4M_1(\gamma+1)\sin\theta\cos\theta)\,\delta M_1 + (2M_1^4 \sin^2\theta((\gamma+1)-2\gamma\sin^2\theta)+2M_1^2((\gamma+1) - 4\sin^2\theta)+4)\,\delta\theta + (M_1^4 \sin^2\theta(4\gamma\sin^2\theta-(\gamma+1)^2)-4M_1^2(\gamma-1)\sin^2\theta-4)\,\delta\omega = 0. \tag{4}$$

The pressure change caused by the reflected isentropic wave is given (Liepmann & Roshko 1957) by

$$\frac{\delta p_3}{p_2} = \frac{\gamma M_2^2}{(M_2^2-1)^{1/2}}\delta\zeta_r. \tag{5}$$

The requirement of matched flow direction on either side of the dividing streamline (equation (1)) allows (5) to be expressed as

$$\frac{\delta p_3}{p_2} = \frac{-\gamma M_2^2}{(M_2^2-1)^{1/2}}\delta\omega. \tag{6}$$

The matched pressure condition (2), may be written

$$\frac{\delta p_4}{p_1} = \frac{\delta p_3}{p_2}\frac{p_2}{p_1}. \tag{7}$$

Combining (3) and (6) and the relationship for the oblique shock pressure ratio with (7) yields the expression

$$4M_1 \sin^2\theta\,\delta M_1 + 4M_1^2 \sin\theta\cos\theta\,\delta\theta + \frac{M_2^2}{(M_2^2-1)^{1/2}}(1-\gamma+2\gamma M_1^2\sin^2\theta)\,\delta\omega = 0. \tag{8}$$

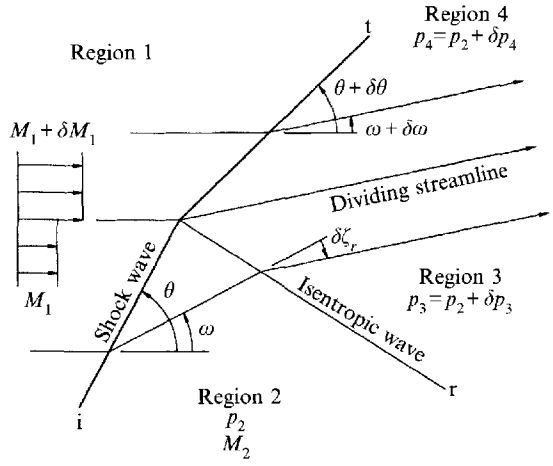

FIGURE 1. Shock wave–Mach number gradient interaction model: i, incident shock; t, transmitted shock; r, reflected isentropic wave.

By eliminating $\delta\omega$ between (4) and (8), the following expression is obtained:

$$\lim_{\delta M_1 \to 0}\left(\frac{\delta\theta}{\delta M_1}\right) = \frac{\partial\theta}{\partial M_1} = f(M_1, \theta)$$

$$= -\{4M_1^5 A \sin^4\theta[4\gamma\sin^2\theta - (\gamma+1)^2] - 8M_1^3\sin^3\theta[\gamma(\gamma+1)\cos\theta + 2A(\gamma-1)\sin\theta]$$
$$-4M_1\sin\theta[4A\sin\theta - (\gamma+1)(\gamma-1)\cos\theta]\}/\{4M_1^6\sin^3\theta[\gamma\sin\theta((\gamma+1) - 2\gamma\sin^2\theta)$$
$$-A\cos\theta(4\gamma\sin^2\theta - (\gamma+1)^2)] + 2M_1^4\sin^2\theta[2\gamma((\gamma+1) - 4\sin^2\theta) - (\gamma-1)(\gamma+1)$$
$$-2\gamma\sin^2\theta) + 8A(\gamma-1)\sin\theta\cos\theta] + 2M_1^2[8A\sin\theta\cos\theta$$
$$+4\gamma\sin^2\theta - (\gamma-1)((\gamma+1) - 4\sin^2\theta)] - 4(\gamma-1)\}, \tag{9}$$

where $$A = (M_2^2 - 1)^{1/2}/M_2^2.$$

Equation (9) is the relationship which determines the change in shock direction due to gradients in the pre-shock Mach number distribution.

In the current model, the major source of shock curvature is the Mach number distribution ahead of the wave, since it is assumed that the shock is generated by a straight oblique wedge at an angle low enough to maintain supersonic flow throughout the flow field. Additional changes in shock direction may occur due to the impingement of post-shock isentropic waves (figure 2). These secondary isentropic waves arise through the interaction of the primary isentropic waves and the post-shock Mach number gradients. However, because the secondary isentropic waves will typically be weaker than primary isentropic waves, the impingement of post-shock isentropic waves will generally have a similar influence on the shock direction than the pre-shock Mach number distribution. Furthermore, if the Mach number remains sufficiently high throughout the mixing region, the oblique angles of the shock wave and the post-shock isentropic waves will result in a large proportion of the shock wave–isentropic wave interaction events occurring after the shock wave has passed through the mixing region. Thus, to a fair approximation, the shock direction within the mixing region may be treated as a function of the pre-shock Mach number alone. That is,

$$\frac{\mathrm{d}\theta}{\mathrm{d}M_1} = f(M_1, \theta). \tag{10}$$

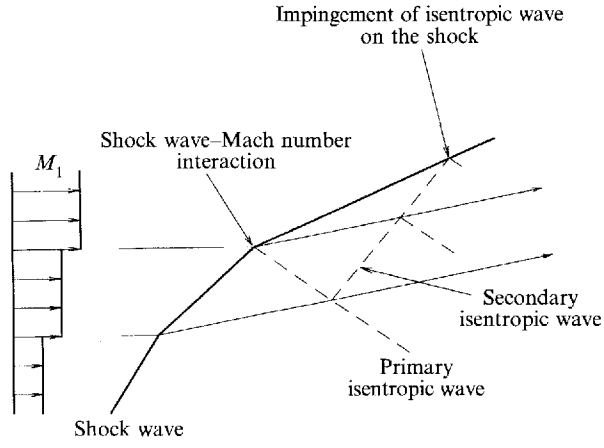

FIGURE 2. Illustration of a post-shock isentropic wave impinging on the oblique shock.

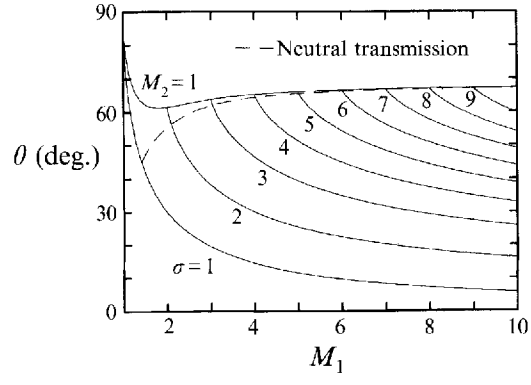

FIGURE 3. Wave angles for shocks of different strengths in a region of varying Mach number, $\gamma = 1.4$.

Given initial values of M_1 and θ it is thus possible to integrate (10) (for a known value of γ) to find the shock angle at any particular Mach number (provided $M_2 > 1$). Having obtained the shock wave angle as a function of the pre-shock Mach number, the shock properties such as pressure ratio, temperature ratio, and flow turning angle may be calculated using the usual oblique shock relations. Furthermore, if the Mach number distribution ahead of the shock, $M_1(y)$ is also available, the shock wave trajectory $\theta(y)$ may be determined. (Alternatively, $M_1(y)$ may be found if $\theta(y)$ is known.)

Results from the integration of (10) are presented in figure 3 for $\gamma = 1.4$ and a number of initial values of M_1 and θ. Each of the shock waves represented has a different 'wave strength', σ, which is a parameter that is currently defined as the pre-shock Mach number at which the post-shock flow becomes sonic. Shock waves which pass through regions of variable Mach number cannot simply be defined in terms of say the pressure or density ratio, because these values change as the shock moves into regions of different Mach number.

As a demonstration of the interpretation of figure 3, consider the shock wave with strength $\sigma = 2$. Such a shock wave will have an angle of approximately 17° at a Mach number of 10. If this same oblique shock wave enters a region of flow with a Mach

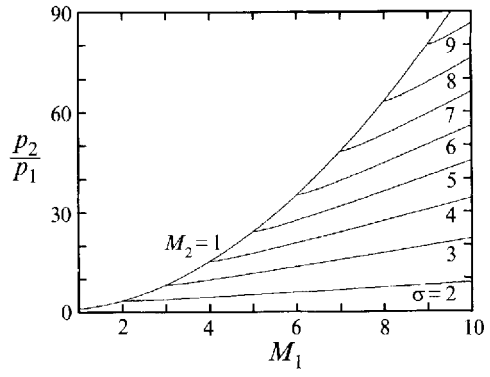

FIGURE 4. Pressure ratios for shocks of different strengths in a region of varying Mach number, $\gamma = 1.4$.

number lower than 10, then for each Mach number, the angle of this shock will be given by the curve $\sigma = 2$ shown in figure 3. For example, if the shock passes into a region where $M_1 = 5$, at this location the shock will have an angle of approximately 25°. If this shock reaches a flow region where $M_1 = 2$, then at this point the shock angle will be approximately 62° and the post-shock flow will be sonic; if the shock enters a flow region with $M_1 < 2$, a subsonic post-shock flow will be produced and no solution is possible with the current method.

The pressure ratios across the shock waves of figure 3 are presented in figure 4; these curves were calculated using the usual oblique shock pressure relationship with $\gamma = 1.4$. Following the values of θ (figure 3) and p_2/p_1 (figure 4) along any of the waves ($\sigma = \text{const.}$) reveals that, generally, lower wave angles and higher pressures will be generated by shocks in higher Mach number regions. This effect is in accord with the well-known weak oblique shock results which dictate that an oblique shock will lie closer to the generating wedge and produce a larger pressure ratio at higher oncoming Mach numbers.

Some straightforward results worth noting are obtained by examining the governing equation in the hypersonic limit ($M_1 \to \infty$). For an oblique shock wave with an angle θ, the post-shock Mach number M_2 approaches a finite, non-zero value as $M_1 \to \infty$. The quantity A in (9) is therefore finite as $M_1 \to \infty$. Since the largest terms in the numerator of (9) are $O(M_1^5)$, whereas the largest terms in the denominator are $O(M_1^6)$, it is clear that $\mathrm{d}\theta/\mathrm{d}M_1 \to 0$ in the hypersonic limit. In other words, as higher Mach numbers are approached, the shock wave direction becomes less sensitive to Mach number changes, as figure 3 clearly illustrates. This result is rational since δM_1 becomes meaningless if $M_1 \to \infty$.

For a given value of γ, certain M_1 and θ combinations will allow the entry of a shock wave into a different Mach number region without generating a reflected isentropic wave. Such a neutral oblique shock transmission situation is analogous to the tailored interface condition in an unsteady reflected shock tunnel. Henderson (1967) obtained the following result for neutral oblique shock transmission in a gas with uniform γ:

$$p_2/p_1 = M_1^2 - 1. \tag{11}$$

Thus, the neutral transmission oblique shock angle is given by

$$\theta = \sin^{-1}\left(\frac{\gamma+1}{2\gamma} - \frac{1}{\gamma M_1^2}\right)^{1/2} \tag{12}$$

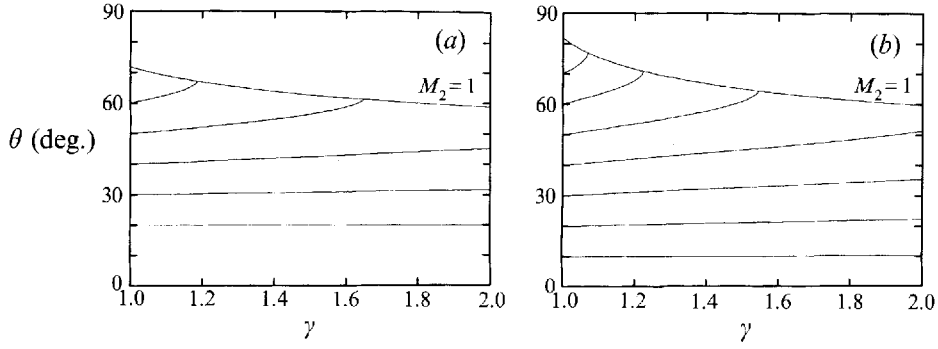

FIGURE 5. Wave angles for shocks of different strengths in a region of varying γ. (*a*) Mach 3 stream, (*b*) Mach 7 stream.

when γ is constant. Using (12), the locus of neutral transmission conditions is plotted in figure 3 for $\gamma = 1.4$. Shock waves will generate isentropic expansion waves as they enter regions of lower Mach number, except when the Mach number is lower (or wave angle is higher) than the neutral value. Conversely, isentropic compression waves will be generated if the shock enters regions of higher Mach number, except when the Mach number is lower (or wave angle is higher) than the neutral value.

2.2. *Effects of mixing between dissimilar gases*

In the previous subsection it was assumed that the ratio of specific heats of the pre-shock mixing region was constant. This is a reasonable assumption for a fuel–air mixing region if the fuel is hydrogen and negligible real gas effects are present in the air, since both streams will have $\gamma \approx 1.4$. However, if a simulated fuel–air mixing region such as that formed between helium ($\gamma = 1.66$) and air is being examined, or a significant fraction of water vapour ($\gamma = 1.33$) is present due to combustion, or if the fuel is a hydrocarbon such as ethane ($\gamma = 1.19$), then a measurable change in γ may be evident, and could affect the transmission of a shock wave through the mixing region.

To assess the effects of a varying-γ region on the shock transmission, an analysis similar to that presented in the previous section was performed (Buttsworth 1994). For the non-uniform γ-distribution analysis, the pre-shock Mach number was treated as a constant so that the final expression analogous to (10) was

$$\frac{\mathrm{d}\theta}{\mathrm{d}\gamma} = q(\gamma, \theta). \tag{13}$$

Given initial values of γ and θ it is thus possible to integrate (13) (for a known value of M_1) to find the shock angle at any particular value of γ (provided $M_2 > 1$). Typical results are presented in figure 5 for $M_1 = 3$ and 7.

The results indicate that an oblique shock wave of moderate strength may experience a significant change in direction if it passes into a flow region with a different γ. For example, consider two shock waves: the first with an angle of approximately 40° in a uniform Mach 3 flow, and the second with an angle of approximately 30° in a uniform Mach 7 flow. Both of these hypothetical shocks will increase their angles by about 5° in passing from a region where $\gamma = 1.0$ to a region where $\gamma = 2.0$. At hypersonic speeds, even a small change in shock angle may induce measurable differences in say, the post-shock pressure. Therefore, under certain extreme conditions, the shock

transmission can be affected by variations in γ. However, for weaker shock waves, or for transverse variations in γ that are more representative of actual scramjet combustor conditions, the effects will be far less severe. For example, figure 5 indicates that a flow region in which γ varies between 1.3 and 1.4 will cause a 30° shock in a Mach 3 flow to change direction by less than 0.2°.

2.3. *Shock-induced changes in mixing characteristics*

Hayes (1957) derived an expression for the vorticity jump across a gasdynamic discontinuity in an inviscid flow. The result obtained by Hayes was more general than previous derivations by Truesdell (1952) and Lighthill (1957) which utilized thermodynamic relationships such as Crocco's vorticity law. No assumptions regarding the thermodynamic properties or composition of the gas were made: the derivation was based on a purely dynamic approach. In the current planar shock wave problem, the equation derived by Hayes for the vorticity jump in steady flow (Hayes, equation 17) may be written

$$\xi_2 = \left(\frac{1}{\rho_2} - \frac{1}{\rho_1}\right)\frac{\partial(\rho_1 u_{1n})}{\partial t} - \frac{u_{1t}}{u_{1n}}\left(\frac{\rho_2}{\rho_1} - 1\right)\frac{\partial u_{1t}}{\partial t} + \xi_1, \tag{14}$$

where n and t refer to the directions normal and tangential to the shock wave.

For the purpose of calculating the vorticity, flow properties along streamlines ahead of the shock are assumed constant. That is, the effects of mixing on the streamwise variation of properties are neglected. The natural coordinate system may therefore be transformed to the Cartesian plane using

$$u_{1n} = u_1 \sin\theta, \quad u_{1t} = u_1 \cos\theta, \quad \frac{\partial}{\partial t} = \sin\theta \frac{\mathrm{d}}{\mathrm{d}y}. \tag{15a–c}$$

In the present case, the pre-shock vorticity, ξ_1, is simply

$$\xi_1 = -\frac{\mathrm{d}u_1}{\mathrm{d}y}. \tag{16}$$

Currently, it is assumed that the effects of post-shock isentropic wave impingement are small and that the influence of any variations in γ can be neglected. Thus, the shock wave direction is determined by the pre-shock Mach number alone. Therefore,

$$\frac{\mathrm{d}\theta}{\mathrm{d}y} = \frac{\mathrm{d}\theta}{\mathrm{d}M_1}\frac{\mathrm{d}M_1}{\mathrm{d}y}. \tag{17}$$

Since velocity and density gradient terms occur in the initial vorticity expression, (14), it is convenient to likewise express the Mach number gradient in terms of these variables. Expanding the Mach number gradient with use of the perfect gas relations yields

$$\frac{\mathrm{d}M_1}{\mathrm{d}y} = \frac{1}{\mathrm{a}_1}\frac{\mathrm{d}u_1}{\mathrm{d}y} + \frac{M_1}{2\rho_1}\frac{\mathrm{d}\rho_1}{\mathrm{d}y} \tag{18}$$

since it has already been assumed that $\mathrm{d}p_1/\mathrm{d}y = 0$. Combining (14)–(18) gives

$$\xi_2 = \left\{\left[\left(\frac{\rho_1}{\rho_2}\right)^{1/2} - \left(\frac{\rho_2}{\rho_1}\right)^{1/2}\right]^2 M_1 \sin\theta\cos\theta\frac{\mathrm{d}\theta}{\mathrm{d}M_1} + 2\left(\frac{\rho_1}{\rho_2} - 1\right)\sin^2\theta - \frac{\rho_1}{\rho_2}\sin^2\theta - \frac{\rho_2}{\rho_1}\cos^2\theta\right\}\frac{\mathrm{d}u_1}{\mathrm{d}y}$$
$$+ \frac{u_1}{2\rho_1}\left\{\left[\left(\frac{\rho_1}{\rho_2}\right)^{1/2} - \left(\frac{\rho_2}{\rho_1}\right)^{1/2}\right]^2 M_1 \sin\theta\cos\theta\frac{\mathrm{d}\theta}{\mathrm{d}M_1} + 2\left(\frac{\rho_1}{\rho_2} - 1\right)\sin^2\theta\right\}\frac{\mathrm{d}\rho_1}{\mathrm{d}y}. \tag{19a}$$

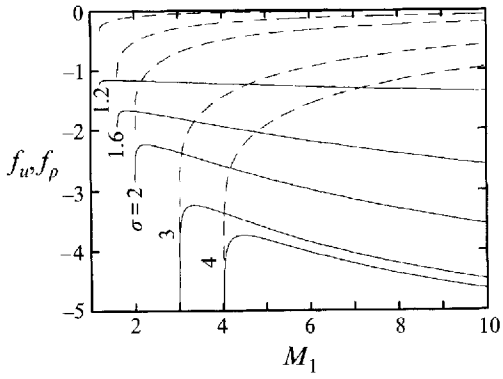

FIGURE 6. Vorticity functions for shocks of different strengths in a region of varying Mach number, $\gamma = 1.4$: ——, f_u; – – –, f_ρ.

To facilitate further discussion of this equation, it is now written as

$$\xi_2 = f_u(M_1, \theta)\frac{\mathrm{d}u_1}{\mathrm{d}y} + \frac{u_1}{2\rho_1} f_\rho(M_1, \theta)\frac{\mathrm{d}\rho_1}{\mathrm{d}y} \tag{19b}$$

where the functions f_u and f_ρ are defined by a direct comparison of (19*a*) and (19*b*).

For various shock waves of different strength, the functions f_u and f_ρ are presented in figure 6. For all shock waves, $f_u < -1$, and $f_\rho < 0$. Therefore, if the pre-shock flow has no density gradients, then vorticity will be amplified. If the pre-shock flow has no velocity gradients, then vorticity will be generated provided density gradients exist in the flow. In general, if both density and velocity gradients exist in the pre-shock flow, the vorticity may be either amplified or attenuated through the shock interaction, depending on the direction and magnitude of the gradients and the values of velocity and density. Provided both the velocity and density gradients lie in the same direction, the vorticity will be amplified. When these gradients lie in opposite directions, the density gradient will work against the amplification of vorticity and attempt to induce a rotation in the opposite sense to the pre-shock vorticity. That is, when the velocity and density gradients oppose each other, it is possible that the vorticity will be attenuated by the shock.

The possibility of vorticity attenuation is now demonstrated for the special case of a uniform Mach number flow. If the pre-shock Mach number is uniform, the velocity and density gradients lie in opposite directions and are related by

$$\frac{\mathrm{d}u_1}{\mathrm{d}y} = -\frac{u_1}{2\rho_1}\frac{\mathrm{d}\rho_1}{\mathrm{d}y}. \tag{20}$$

In a uniform Mach number flow, the shock generated by a wedge will be straight. Thus, (19) may be written

$$\xi_2 = \left(\frac{\rho_1}{\rho_2}\sin^2\theta + \frac{\rho_2}{\rho_1}\cos^2\theta\right)\xi_1. \tag{21}$$

The above expression can also be obtained from a consideration of stream tube compression due to a straight oblique shock and applies even when the post-shock flow is subsonic (Buttsworth 1994). The values of ξ_2/ξ_1 predicted by (21), are plotted in figure 7 for various pre-shock Mach numbers. Figure 7 reveals that the pre-shock vorticity may either be amplified or attenuated by the shock wave. By rearranging (19) in terms of the pre-shock vorticity and Mach number gradients (i.e. utilizing (18)), it

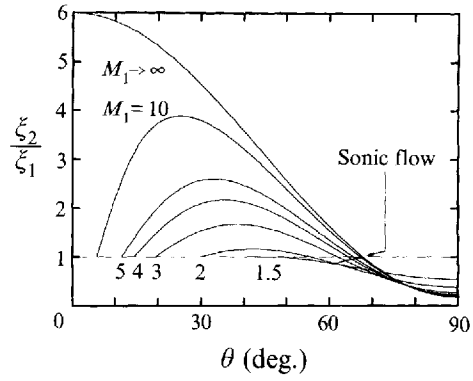

FIGURE 7. Vorticity amplification and attenuation by straight shock waves, $\gamma = 1.4$.

can be observed that in the hypersonic limit, the vorticity amplification will also be given by (21). This is a rational result because as $M_1 \to \infty$, $\mathrm{d}\theta/\mathrm{d}M_1 \to 0$, meaning that the shock wave must be straight. Vorticity amplification results for the hypersonic limit are also presented in figure 7.

3. Applications of the interaction model

3.1. *Mixing augmentation*

While shock waves may locally induce a significant amount of mixing through unsteady mechanisms such shock oscillations and shock–turbulence interactions (e.g. Kumar *et al.* 1989), further downstream the mixing rate is likely to be governed in part by the large-scale post-shock vorticity. For example, Shau & Dolling (1992) observed an increase in the turbulent activity through shock impingement on a shear layer; however, such augmentation was found to rapidly decay downstream of the shock impingement location. The current analysis presents a means of calculating the steady component of the post-shock vorticity and thus provides a guide to the possible mixing augmentation that may persist after the unsteady mixing enhancement effects have decayed.

During scramjet powered flight at Mach numbers lower than approximately 12, the fuel (hydrogen) is likely to be injected as a jet which moves at a speed in excess of the air velocity (Anderson, Kumar & Erdos 1990). At flight Mach numbers higher than approximately 12, the fuel is likely to form a wake (i.e. fuel injection at speeds lower than the air velocity). Since the injected hydrogen will be less dense than the combustor air stream, the gradients of density and velocity will typically be aligned only when the fuel is injected at a speed lower than the surrounding air. Therefore, the vorticity in the mixing region would be amplified through a shock wave interaction in the wake flow case ($M_\infty > 12$). If the fuel and the air are flowing at the same velocity ($M_\infty \approx 12$), increased vorticity may result from shock wave impingement. However, in the jet flow case ($M_\infty < 12$), the velocity and density gradients will be misaligned. This misalignment does not immediately imply that the vorticity will be attenuated by the shock; however, it does indicate that the components of the shock-induced vorticity associated with the density and the velocity fields will counteract each other. Thus, at the higher flight speeds ($M_\infty > 12$), shock impingement may augment mixing, whereas at the lower speeds ($M_\infty < 12$), shock impingement is likely to be less efficient and may even attenuate the mixing.

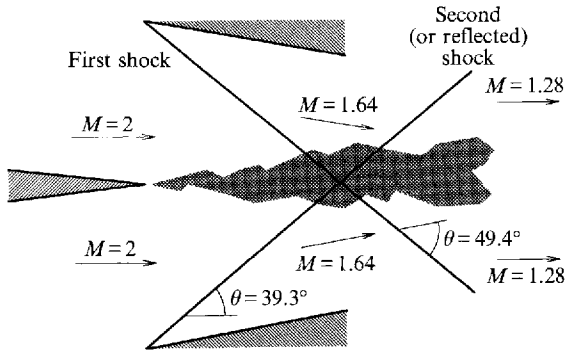

FIGURE 8. Schematic representation of the symmetric 10° wedge shock-induced mixing configuration studied by Drummond *et al.* (1991).

Drummond, Carpenter & Riggins (1991) examined the effects of shock impingement on a mixing layer formed between two streams both at Mach 2, but moving at different velocities. In the calculations performed by Drummond and his colleagues, two shocks, each with a turning angle of 10°, entered the mixing layer symmetrically from each side as shown in figure 8. Using the free-stream conditions reported by Drummond *et al.* (1991), and the assumption that the local total enthalpy is a linear function of the mixing layer velocity (Hayes & Probstien 1959), it is estimated that the minimum Mach number within the mixing layer was 1.92. For $M_1 = 2$ and $\theta = 39.3°$ (corresponding to a 10° turning angle shock), (10) gives $\mathrm{d}\theta/\mathrm{d}M_1 = -21.82°$ (for $\gamma = 1.4$). Thus, it is estimated that the shock direction changed by less than 2° during its traverse of the mixing layer. Therefore, according to the current predictions, the shocks that pass through this layer will be approximately straight, in which case the post-shock vorticity will be given by (21).

According to the present calculations, the first shocks which impinge on the mixing layer will amplify the vorticity by a factor of 1.15 (read off ξ_2/ξ_1 in figure 7 on the curve $M_1 = 2$ at $\theta = 39.3°$). From oblique shock calculations, the flow Mach number behind the first shocks was 1.64 and the angle of the second shocks (relative to the oncoming flow direction) was 49.4°. At these conditions, the second shocks will amplify the vorticity by a factor of only 1.01. Using the present analysis, it is concluded that very little vorticity was gained through the action of the reflected (or second) shocks, and had further straight oblique shocks processed the mixing layer, the vorticity would probably have been attenuated. The current predictions indicate that the net shock-induced vorticity amplification was only 16% which explains why Drummond *et al.* (1991) observed very little mixing augmentation and why they found it necessary to use a curved shock generated by a blunt body in order to amplify the vorticity and thus enhance the mixing. Additional shock curvature (and thus vorticity) may be generated in other mixing layers without resorting to blunt bodies, provided a significant Mach number gradient exists within the mixing region.

3.2. *Oscillating shock waves*

Kumar *et al.* (1989) numerically simulated wall region induced shock oscillations by imposing a periodic Mach number distribution in the wall region upstream of a 10° compression corner. The periodic Mach number distribution was given by

$$M_1(y, t) = M_\infty(1 + \epsilon \sin 2\pi ct), \tag{22}$$

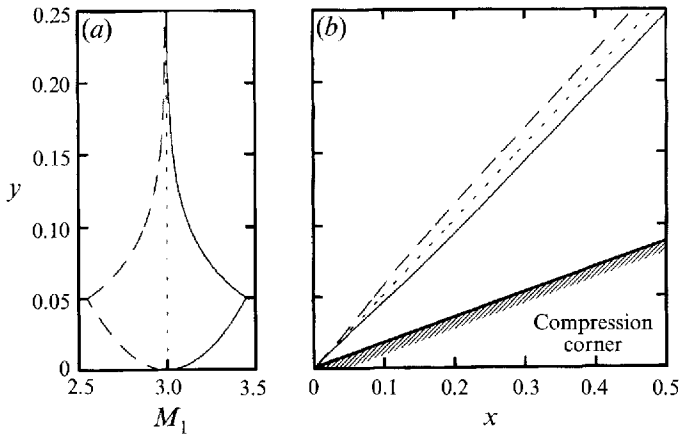

FIGURE 9. (*a*) Mach number distributions and (*b*) shock trajectories for $t = 1/4c$ (——), $1/2c$(----), and $3/4c$ (– – –) in the oscillating shock wave problem.

where $$M_\infty = 3$$

and $$\epsilon = \begin{cases} (0.45y)^{1/2} & \text{for} \quad y < 0.05 \\ 0.15\,\mathrm{e}^{-25(y-0.05)} & \text{for} \quad y > 0.05. \end{cases}$$

The steady analysis presented in the current study was used to provide a solution for the Kumar *et al.* oscillating shock problem which applies in the limit of an infinite oscillation period.

By integrating (10) using $\gamma = 1.4$ and the initial conditions $M_1 = 3$ and $\theta = 27.4°$ (which corresponds to a turning angle of 10°), the instantaneous shock trajectory (in the limit of an infinite oscillation period) may be determined using the above Mach number distribution (see figure 9). For the present analysis, the oscillation period was divided into 40 time steps; the shock trajectory and post-shock velocities were determined at each step. The calculation of the velocities downstream of the shock was simplified by (i) neglecting the small accelerations due to the post-shock isentropic waves; and (ii) treating all the post-shock streamlines as moving in a direction parallel to the wedge. The quantities and $\overline{u'v'}$ and $\frac{1}{2}(\overline{u'^2}+\overline{v'^2})$ were then obtained for $y = 0.065$ and 0.25 by the appropriate averaging over the oscillation period. Results obtained from this procedure are presented in figure 10; the results obtained by Kumar *et al.* are included for comparison.

Kumar *et al.* found that the disturbances generated in the wall region propagated along the shock to produce a curved oscillating shock in the free-stream region ($y > 0.25$, approximately). In the current calculations, the wall region disturbances do affect the shock location (figure 9); however, the free-stream shock remains straight. The present shock oscillation region (see figure 10) is characterized by a relatively flat distribution of normalized Reynolds stress and lies upstream of the Kumar *et al.* predictions. The finite shock thickness calculated in the numerical scheme of Kumar *et al.* may contribute to these differences. From the results presented by Kumar *et al.*, the steady shock wave thickness was estimated to be 0.05 units in the x-direction. Since this thickness is comparable to the maximum shock distance, shock smearing is likely to have affected their results. As the shock oscillation frequency decreases, the Kumar *et al.* results indicate that, for locations within the shock oscillation region, the magnitude of the normalized Reynolds stress increases. The present results suggest that this trend does not continue to the limit of an infinite oscillation period. That is, for the

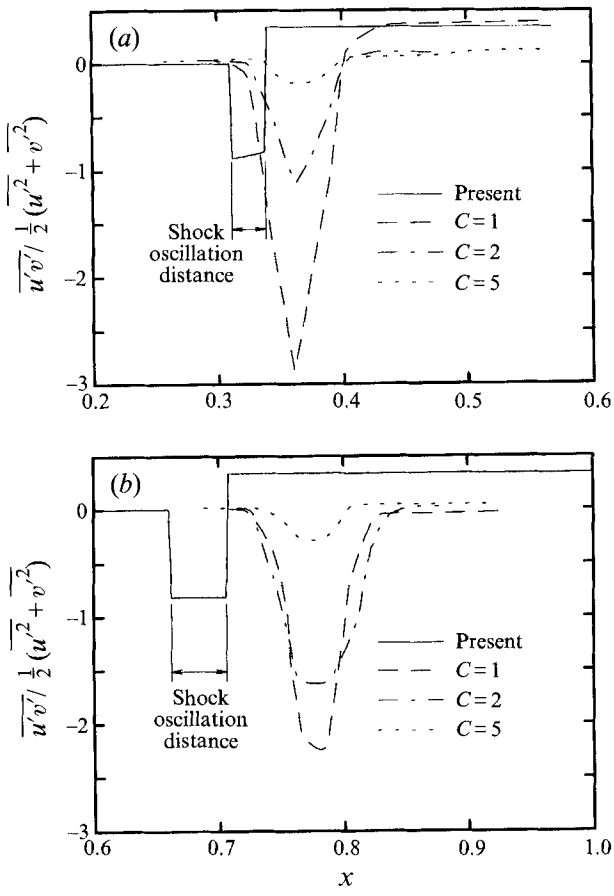

FIGURE 10. Normalized time-averaged Reynolds stress production by the oscillating shock at (*a*) $y = 0.065$ and (*b*) 0.25: ——, present results; – –, results from Kumar *et al.* (1989).

configuration examined, the maximum value of normalized Reynolds stress will be generated at a finite (non-zero) shock oscillation frequency.

4. Conclusion

The interaction of an oblique shock with a planar supersonic mixing region was modelled using difference forms of the Rankine–Hugoniot equations. A differential equation describing the shock trajectory due to gradients in the pre-shock Mach number was obtained. The impingement of post-shock isentropic waves on the shock wave, and variations in the ratio of specific heats across the mixing region, can influence the shock trajectory; however, these effects are frequently small. When such effects can be neglected, the shock trajectory becomes a function only of the Mach number distribution within the mixing region. The equation governing the shock trajectory due to the Mach number gradients was integrated for a number of different shocks. Shock pressure ratio and vorticity results are also presented for a number of shocks.

It was found that the pre-shock vorticity will not necessarily be amplified through the shock interaction. For the special case of straight shock waves, the vorticity is likely

to be attenuated when the post-shock Mach number approaches unity. In the more general case of a mixing region with significant Mach number variations, vorticity will be amplified if the velocity and density lie in the same direction, but may be attenuated if they lie in opposite directions. Thus, for scramjets, shock-induced mixing enhancement may be more effective at the higher flight speeds since the velocity and density gradients within the mixing region are typically aligned at the higher speeds. The use of the present vorticity analysis as a means of assessing proposed shock impingement configurations was demonstrated by predicting the mixing augmentation (based on vorticity amplification) for a published shock wave–mixing layer simulation. Other aspects of the present shock analysis were demonstrated through the calculation of an oscillating shock configuration (in the limit of an infinite oscillation period). From a comparison with previous numerical shock oscillation results, it appears that there exists a finite (non-zero) shock oscillation frequency at which the production of relative turbulent stress will be greatest.

The author wishes to acknowledge the financial support provided by an Australian Postgraduate Research Award and NASA through grant NAGW-674.

REFERENCES

ANDERSON, G., KUMAR, A. & ERDOS, J. 1990 Progress in hypersonic combustion technology with computation and experiment. *AIAA Paper* 90-5254.

ANYIWO, J. C. & BUSHNELL, D. M. 1982 Turbulence amplification in shock-wave boundary layer interaction. *AIAA J.* **20**, 893–899.

BUTTSWORTH, D. R. 1994 Shock induced mixing and combustion in scramjets. PhD thesis, Department of Mechanical Engineering, The University of Queensland.

DRUMMOND, J. P. 1991 Mixing enhancement of reacting parallel fuel jets in a supersonic combustor. *AIAA Paper* 91-1914.

DRUMMOND, J. P., CARPENTER, M. H. & RIGGINS, D. W. 1991 Mixing and mixing enhancement in supersonic reacting flowfields. In *High-Speed Flight Propulsion Systems* (ed. S. N. B. Murthy & E. T. Curran). Progress in Astronautics and Aeronautics, vol. 137, pp. 383–455. AIAA.

FERNANDO, E. M. & MENON, S. 1993 Mixing enhancement in compressible mixing layers: an experimental study. *AIAA J.* **31**, 278–285.

GILREATH, H. E. & SULLINS, G. A. 1989 Investigation of the mixing of parallel supersonic streams. *ISABE Paper* 89-7060.

GUIRGUIS, R. H. 1988 Mixing enhancement in supersonic shear layers: III. Effect of convective Mach number. *AIAA Paper* 88-0701.

HALL, J. L., DIMOTAKIS, P. E. & ROSEMAN, H. 1993 Experiments in nonreacting compressible shear layers. *AIAA J.* **31**, 2247–2254.

HAYES, W. D. 1957 The vorticity jump across a gasdynamic discontinuity. *J. Fluid Mech.* **2**, 595–600.

HAYES, W. D. & PROBSTIEN, R. F. 1959 *Hypersonic Flow Theory*, 1st edn. Academic Press.

HENDERSON, L. F. 1967 The reflexion of a shock wave at a rigid wall in the presence of a boundary layer. *J. Fluid Mech.* **30**, 699–722.

HYDE, C. R., SMITH, B. R., SCHETZ, J. A. & WALKER, D. A. 1990 Turbulence measurements for heated gas slot injection in supersonic flow. *AIAA J.* **28**, 1605–1614.

KUMAR, A., BUSHNELL, D. M. & HUSSAINI, M. Y. 1989 Mixing augmentation technique for hypervelocity scramjets. *J. Propulsion Power* **5**, 514–522.

LI, C., KAILASANATH, K. & BOOK, D. L. 1991 Mixing enhancement by expansion waves in supersonic flows of different densities. *Phys. Fluids* A **3**, 1369–1373.

LIEPMANN, H. W. & ROSHKO, A. 1957 *Elements of Gasdynamics*. Wiley.

LIGHTHILL, M. J. 1957 Dynamics of a dissociating gas. Part 1. Equilibrium flow. *J. Fluid Mech.* **2**, 1–32.

MARBLE, F. E., HENDRICKS, G. J. & ZUKOSKI, E. E. 1987 Progress toward shock enhancement of supersonic combustion processes. *AIAA Paper* 87-1880.

MARBLE, F. E., ZUKOSKI, E. E., JACOBS, J. W. & HENDRICKS, G. J. 1990 Shock enhancement of and control of hypersonic mixing and combustion. *AIAA Paper* 90-1981.

MENON, S. 1989 Shock-wave-induced mixing enhancement in scramjet combustors. *AIAA Paper* 89-0104.

MCKENZIE, J. F. & WESTPHAL, K. O. 1968 Interaction of linear waves with oblique shocks. *Phys. Fluids* **11**, 2350–2362.

MORKOVIN, M. V. 1960 Note on the assessment of flow disturbances at a blunt body travelling at supersonic speeds owing to flow disturbances in free stream. *Trans ASME* E: *J. Appl. Mech.* **27**, 223–229.

NORTHAM, G. B. & ANDERSON, G. Y. 1986 Supersonic combustion ramjet research at Langley. *AIAA Paper* 86-0159.

NORTHAM, G. B., CAPRIOTTI, D. P., BYINGTON, C. S. & GREENBERG, I. 1991 Supersonic mixing and combustion in scramjets. *ISABE Paper* 91-7095.

RANDOLPH, H., CHEW, L. & JOHARI, H. 1994 Pulsed jets in supersonic crossflow. *J. Propulsion Power* **10**, 746–748.

RIBNER, H. S. 1987 Spectra of noise and amplified turbulence emanating from shock-turbulence interaction. *AIAA J.* **25**, 436–442.

RILEY, N. 1959 Interaction of a shock wave with a mixing region. *J. Fluid Mech.* **7**, 321–339.

ROSHKO, A. & THOMKE, G. J. 1970 Supersonic, turbulent boundary-layer interaction with a compression corner at very high Reynolds number. In *Viscous Interaction Phenomena in Supersonic and Hypersonic Flow*, pp. 109–138. University of Dayton Press, Ohio.

ROY, G. D. 1991 Subsonic and supersonic mixing and combustion enhancement. *ISABE Paper* 91-7093.

SCHADOW, K. C., GUTMARK, E. & WILSON, K. J. 1990 Compressible spreading rates of supersonic coaxial jets. *Exps. Fluids* **10**, 161–167.

SHAU, Y. R. & DOLLING, D. S. 1992 Exploratory study of turbulent structure of a compressible shear layer using fluctuating Pitot pressure measurements. *Exps. Fluids* **12**, 293–306.

SHAU, Y. R., DOLLING, D. S. & CHOI, K. Y. 1993 Organized structure in a compressible turbulent shear layer. *AIAA J.* **31**, 1398–1405.

SULLINS, G. A., GILREATH, H. E., MATTES, L. A., KING, P. S. & SCHETZ, J. A. 1991 Instabilities in confined supersonic mixing layers. *ISABE Paper* 91-7096.

TILLMAN, T. G., PATRICK, W. P. & PATERSON, R. V. 1991 Enhanced mixing of supersonic jets. *J. Propulsion Power* **7**, 1006–1014.

TRUESDELL, C. 1952 On curved shocks in steady plane flow of an ideal fluid. *J. Aero. Sci.* **19**, 826–828.

VASILEV, V. I., ZAKOTENKO, S. N., KRASKENINNIKOV, S. JU. & STEPANOV, V. A. 1994 Numerical investigation of mixing augmentation behind oblique shock waves. *AIAA J.* **32**, 311–316.

WAITZ, I. A., MARBLE, F. E. & ZUKOSKI, E. E. 1993 Investigation of a contoured wall injector for hypervelocity mixing augmentation. *AIAA J.* **31**, 1014–1021.

YANG, J., KUBOTA, T. & ZUKOSKI, E. E. 1993 Applications of shock-induced mixing to supersonic combustion. *AIAA J.* **31**, 854–862.